RESEARCH

# Vinculin strengthens the endothelial barrier during vascular development

**Miesje M van der Stoel[1,*], Maria P Kotini[2,*], Rianne M Schoon[1], Markus Affolter[2], Heinz-Georg Belting[2,†] and Stephan Huveneers[1,†]**

[1]Amsterdam UMC, University of Amsterdam, location AMC, Amsterdam Cardiovascular Sciences, Department of Medical Biochemistry, Meibergdreef, Amsterdam, The Netherlands
[2]Biozentrum der Universität Basel, Spitalstrasse, Basel, Switzerland

**Correspondence should be addressed to H Belting or S Huveneers: heinz-georg.belting@unibas.ch or s.huveneers@amsterdamumc.nl**

*(M M van der Stoel and M P Kotini contributed equally to this work)
†(H-G Belting and S Huveneers contributed equally as senior authors)

## Abstract

Remodelling of cell–cell junctions is crucial for proper tissue development and barrier function. The cadherin-based adherens junctions anchor via β-catenin and α-catenin to the actomyosin cytoskeleton, together forming a junctional mechanotransduction complex. Tension-induced conformational changes in the mechanosensitive α-catenin protein induce junctional vinculin recruitment. In endothelial cells, vinculin protects the remodelling of VE–cadherin junctions. In this study, we have addressed the role of vinculin in endothelial barrier function in the developing vasculature. *In vitro* experiments, using endothelial cells in which α-catenin was replaced by a vinculin-binding-deficient mutant, showed that junctional recruitment of vinculin promotes endothelial barrier function. To assess the role of vinculin within blood vessels *in vivo*, we next investigated barrier function in the vasculature of *vcl* knockout zebrafish. In the absence of vinculin, sprouting angiogenesis and vessel perfusion still occurred. Intriguingly, the absence of vinculin made the blood vessels more permeable for 10 kDa dextran molecules but not for larger tracers. Taken together, our findings demonstrate that vinculin strengthens the endothelial barrier and prevents vascular leakage in developing vessels.

**Keywords**

- vinculin
- endothelial barrier
- mechanotransduction
- adherens junction
- zebrafish
- vascular leakage
- extravasation

## Introduction

The semi-permeable vascular barrier between the blood and the surrounding tissue is maintained by a monolayer of endothelial cells (1). The endothelial barrier regulates the extravasation of leukocytes and fluid (2, 3). Changes in permeability induced by angiogenic growth factors or inflammatory cytokines are often temporal and reversible, ensuring recovery of the vascular barrier (4). Chronic disruptions of the endothelial barrier however, perturb vascular homeostasis and contribute to a multitude of pathologies, including atherosclerosis, cancer and inflammatory diseases (1, 5). Hence, maintaining a tight, yet adaptable, endothelial barrier is important.

The endothelium in the developing vasculature is exposed to multiple forces that are derived from the mural cells, blood pressure and hemodynamic forces from the bloodstream (6, 7, 8, 9). Endothelial cells sense and transmit such mechanical cues via their cell–cell contacts, which evoke proportional cellular responses to maintain the endothelial barrier (10). VE–cadherin-based adherens

https://vb.bioscientifica.com
https://doi.org/10.1530/VB-22-0012

junctions (AJs) are crucial adhesion structures that form endothelial cell–cell contacts (11, 12). Endothelial junction remodelling is required for collective endothelial migration during sprouting angiogenesis (13, 14). The cytoplasmic domain of the transmembrane VE–cadherin protein binds to β-catenin and α-catenin, which in turn couples to the actomyosin cytoskeleton and forms the core junctional mechanotransduction complex (15, 16, 17, 18). The interaction of the VE–cadherin–catenin complex with the actin cytoskeleton stabilises the AJs and maintains endothelial monolayer integrity (19, 20, 21).

Tension on the VE–cadherin complex results in unfolding of α-catenin, which enhances its actin-binding affinity and exposes a cryptic binding site for vinculin (16, 22, 23, 24, 25, 26, 27). The vinculin–α-catenin interaction drives α-catenin-mediated mechanotransduction and preserves junctional integrity during force-dependent remodelling in cultured endothelial and epithelial cells (22, 25, 28, 29, 30, 31). Vinculin recruitment to AJs occurs to different extents during agonist-induced endothelial barrier enhancing and disrupting processes (22, 32, 33). In zebrafish embryos, vinculin associates with endothelial junctions that are remodelled by changes in blood flow (34) and endothelial expression of vinculin is important for angiogenesis in the postnatal mouse retina (35). Whether junctional vinculin has a role in endothelial barrier function remains unclear.

In this study, we found that junctional vinculin recruitment facilitates endothelial barrier function *in vitro*. To define the importance of vinculin for endothelial tissue integrity in vivo, we examined the vasculature of *vcl*-knockout zebrafish. We found that the endothelial cells still generated a functional and perfused vasculature in the absence of vinculin. Interestingly, the developed blood vessels in *vcl* mutant zebrafish were more permeable for small dextran molecules, whereas large dextran molecules did not extravasate. Taken together, these results point to a role for vinculin in strengthening the endothelial barrier in the vasculature.

## Materials and methods

### Antibodies and reagents

Rabbit polyclonal anti-VE–cadherin (Cat# 36-1900, diluted 1:200 for immunofluorescence (IF)) was from Thermo Fischer Scientific. Purified mouse anti-vinculin (clone hVIN-1, Cat# V9131, diluted 1:400 for IF) was from Sigma Aldrich. Rabbit polyclonal anti-β-actin (Cat# 4867S, diluted 1:1000 for Western blot (WB)) and rabbit polyclonal anti-phospho-paxillin-Tyr118 (Cat# 69363, diluted 1:200 for IF) were from Cell Signaling. Mouse monoclonal anti-α-catenin (Cat# 13-9700; diluted 1:1000 for WB) was from Invitrogen/Zymed and mouse monoclonal anti-GFP (B-2, Cat# sc-9996, diluted 1:1000 for WB) was from Santa Cruz Biotechnology. Promofluor 415 Phalloidin (Promokine, Cat# PK-PF415-7-01, diluted 1:200 for IF) was used for IF of F-actin. Alexa Fluor 488 or 594-coupled secondary antibodies were from Invitrogen (diluted 1:250 for IF). Secondary antibodies coupled to horseradish peroxidase (HRP) were from Bio-Rad (diluted 1:1000 for WB). Human plasma-derived thrombin (used at 1 U/mL) was purchased from Sigma–Aldrich.

### Cell culture

Pooled primary human umbilical vein endothelial cells (HUVECs) from different donors (Lonza) were cultured in endothelial cell growth medium 2 (EGM-2) culture medium supplemented with the growth medium 2 supplement pack (PromoCell) on gelatin-coated tissue flasks. HEK293T cells (ATCC) were cultured in Dulbecco's modified Eagle's medium with L-glutamine and supplemented with 10% FCS and 1% pen/strep. Cells were recently authenticated and tested for contamination.

### DNA plasmids and lentivirus production

To silence α-catenin expression in HUVECs, pLKO.1-shRNA plasmid targeting human α-catenin mRNA was used (TRCN0000062653). ShC002 was used as shRNA control (Sigma–Aldrich mission library). The mouse α-catenin–GFP and α-catenin–ΔVBS–GFP lentiviral plasmids were previously described (22). Lentivirus was generated by transfecting HEK293T cells with the lentiviral expression plasmids and third-generation packaging plasmids using Trans-IT-LTI transfection reagents (Mirus) as described previously (42). To transduce HUVECs, the supernatant containing the lentiviral particles was mixed at a 5:1 ratio with EGM-2 and incubated with the HUVECs for 16 h. Subsequently, transduced HUVECs were selected for expression of the shRNA with 2.5 µg/mL puromycin (Sigma). shRNA-based knockdown levels were analysed at least 72 h after transduction.

### ECIS

To measure endothelial barrier resistance, we used electric-cell impedance sensing as previously described (43). Gold electrode arrays (8W10E, Applied Biophysics) were

https://vb.bioscientifica.com
https://doi.org/10.1530/VB-22-0012

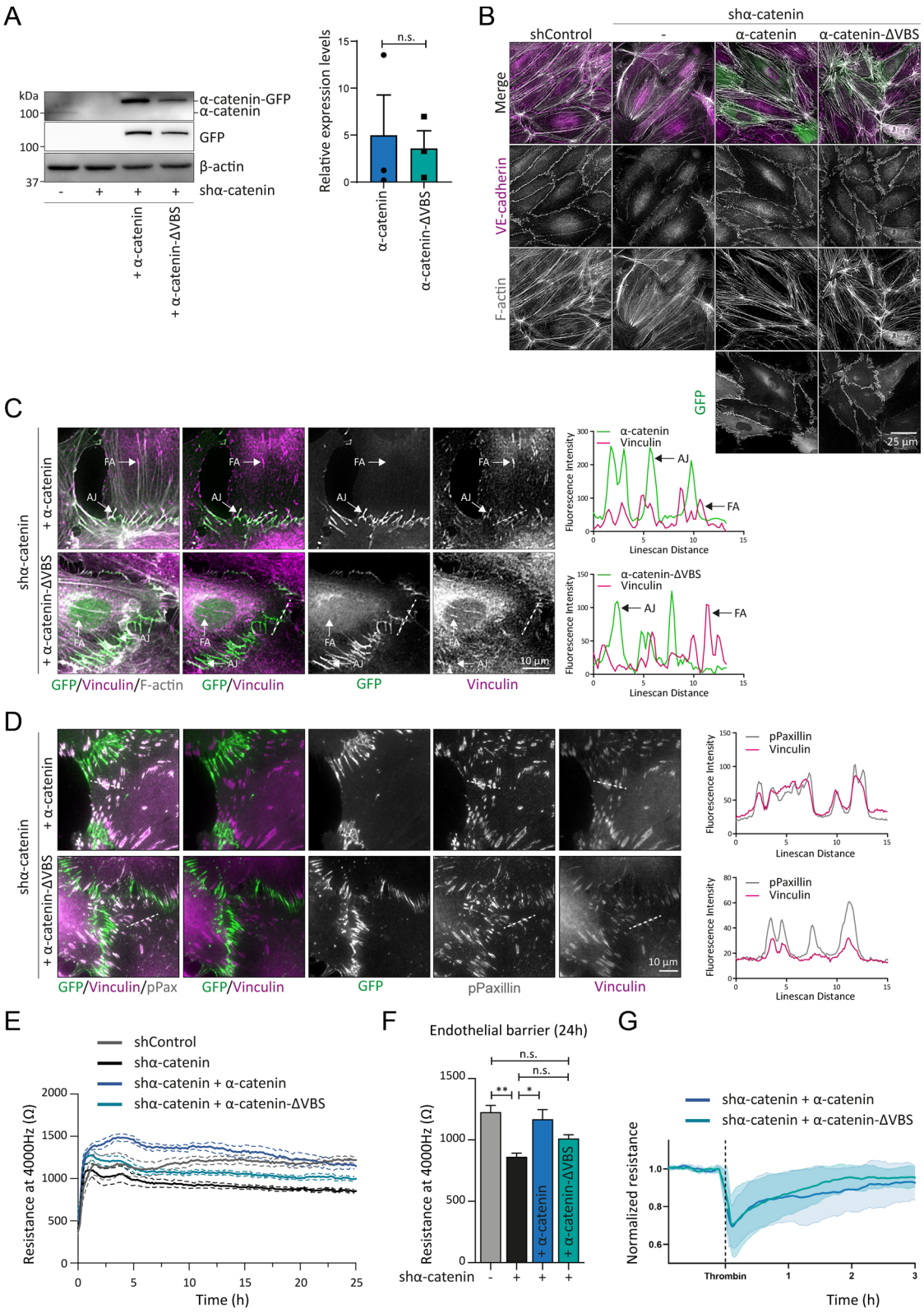


**Figure 1**

Junctional vinculin strengthens the endothelial barrier in vitro. (A) Representative Western blot analysis of shControl and shα-catenin transduced HUVECs rescued with lentiviral expression of α-catenin–GFP or α-catenin–ΔVBS–GFP. Blotted for α-catenin, GFP or β-actin. Bar graphs indicate the average ± s.e. expression levels of α-catenin–GFP and α-catenin–ΔVBS–GFP in shα-catenin-transduced HUVECs relative to endogenous α-catenin levels in shControl

https://vb.bioscientifica.com
https://doi.org/10.1530/VB-22-0012

**Figure 1** (Continued)

HUVECs. n.s., non-significant (non-parametric Wilcoxon matched-pairs signed-rank test). Data are from three independent experiments. (B) Representative immunofluorescent images of shControl and shα-catenin-transduced HUVECs rescued with lentiviral expression of α-catenin–GFP or α-catenin–ΔVBS–GFP. Stained for F-actin (grey) and VE-cadherin (magenta). (C) Representative IF images of shα-catenin HUVECs rescued with α-catenin–GFP or α-catenin–ΔVBS–GFP (green) that were stained for vinculin (magenta) and F-actin (grey). Colocalisation of vinculin with α-catenin–GFP or α-catenin–ΔVBS–GFP was analysed by line scans displaying signal intensity (arbitrary units) across the AJs and FAs as indicated. Scale bar, 10 µm. (D) Representative IF images of shα-catenin HUVECs rescued with α-catenin–GFP or α-catenin–ΔVBS–GFP (green) that were stained for vinculin (magenta) and phosphor-Paxillin Tyr118 (grey). Colocalisation of vinculin with pPaxillin was analysed by line scans displaying signal intensity (arbitrary units) across FAs as indicated. Scale bar, 10 µm. (E) Line graph showing the average resistance ± S.E. measured with ECIS at 4000 Hz of indicated endothelial monolayers over time. Data are from three independent experiments. (F) Bar graphs representing the average resistance ± S.E. measured with ECIS at 4000 Hz of indicated endothelial monolayers after 24 h. Data are from three independent experiments. n.s., non-significant, $^{*}P < 0.05$, $^{**}P < 0.01$, $^{***}P < 0.001$ (one-Way ANOVA with Tukey's post hoc test for multiple comparisons). (G) Line graph showing the average resistance ± S.D. measured with ECIS at 4000 Hz of indicated endothelial monolayers over time following treatment with the permeability factor thrombin. Data are normalised to the baseline values prior to thrombin treatment and are derived from two independent experiments.

treated with 10 mM L-cysteine (Sigma) for 15 min at room temperature. After washing with MQ water, the wells were coated with 5 µg/mL fibronectin in MQ for 1 h at 37°C and 5% $CO_2$. Subsequently, 120,000 cells per well were seeded on the arrays and the impedance was measured during monolayer formation at 4000 Hz using the ECIS model ZTheta (Applied BioPhysics).

## Immunofluorescence stainings

For immunofluorescence stainings, HUVECs were cultured on 5 µg/mL fibronectin-coated coverslips and later fixed for 15 min at room temperature with 4% paraformaldehyde in PBS$^{++}$ (PBS supplemented with 1 mM $CaCl_2$ and 0.5 mM $MgCl_2$). The fixed cells were permeabilised for 5 min at room temperature with 0.5% Triton X-100 in PBS and blocked for 15 min in 2% BSA in PBS. Primary and secondary antibodies were diluted in 0.5% BSA in PBS and incubated for 45 min. Between incubations, fixed cells were washed three times with 0.5% BSA in PBS. Coverslips were mounted in Mowiol4-88/DABCO solution (Sigma).

## Immunoblot analysis

HUVECs were lysed using reduced sample buffer containing 4% β-mercaptoethanol. Samples were denatured at 95°C for 5 min and subsequently loaded on a 10% SDS page gel. Gel running was performed in SDS-page running buffer (25 mM Tris–HCl, pH 8.3, 192 mM glycine and 0.1% SDS) and blotted on ethanol-activated PVDF membranes using full-wet transfer blot buffer (25 mM Tris–HCl, pH 8.3, 192 mM glycine and 20% (v/v) ethanol). Blots were blocked in 5% milk powder in tris-buffered saline (TBS) for 30 min and subsequently incubated with the primary antibodies in 5% milk powder in TBS supplemented with Tween-20 (TBS-t) overnight at 4°C. The secondary antibodies, coupled to HRP, were incubated for 45 min at room temperature. Between antibody incubations, blots were washed three times with TBS-t. As a final step before visualisation, blots were washed one time with TBS. HRP signal was visualised using enhanced chemiluminescence (ECL) detection (Supersignal West Pico PLUS, Thermo Fischer) with an ImageQuant LAS 4000 (GE Healthcare).

## Zebrafish lines and maintenance

Zebrafish were maintained in standard housing conditions according to FELASA guidelines (44). All experiments were performed in accordance with federal guidelines and were approved by the Kantonales Veterinäramt of Kanton Basel-Stadt (1027H, 1014HE2, 1014G). The vcla$^{hu10818}$ ; vclb$^{hu11202}$ zebrafish lines (38) were crossed into the transgenic *Tg(fli1a:EGFP)*$^{y1}$ line, which labels all endothelial cells (45) as described in (34).

## Genotyping of the vinculin (*vcl*)-mutant lines

For genotyping of the vinculin-mutant alleles, genomic DNA was extracted from adult fish fin biopsies or from whole embryos using a standard protocol (46) with addition of proteinase K to the sample. The extracted genomic DNA was then used to genotype the *vcla* and *vclb* loci. Genotyping protocol for *vcla* or *vclb* alleles was performed as described previously (34).

## Microangiography

48 hpf zebrafish embryos were anaesthetised with 1× tricaine (0.08%, Sigma) and were injected with 250 µg/mL of 10 kDa or 70 kDa rhodamine-dextran (Molecular Probes) in the duct of Cuvier using glass needles (Biomedical Instruments) and standard microinjection protocols (47, 48). The injected embryos were transferred back to embryo media (5 mM NaCl, 0.17 mM KCl, 0.33 mM $CaCl_2$, 0.33 mM $MgSO_4$, pH 7.4) to recover and subsequently imaged 1 h

https://vb.bioscientifica.com
https://doi.org/10.1530/VB-22-0012

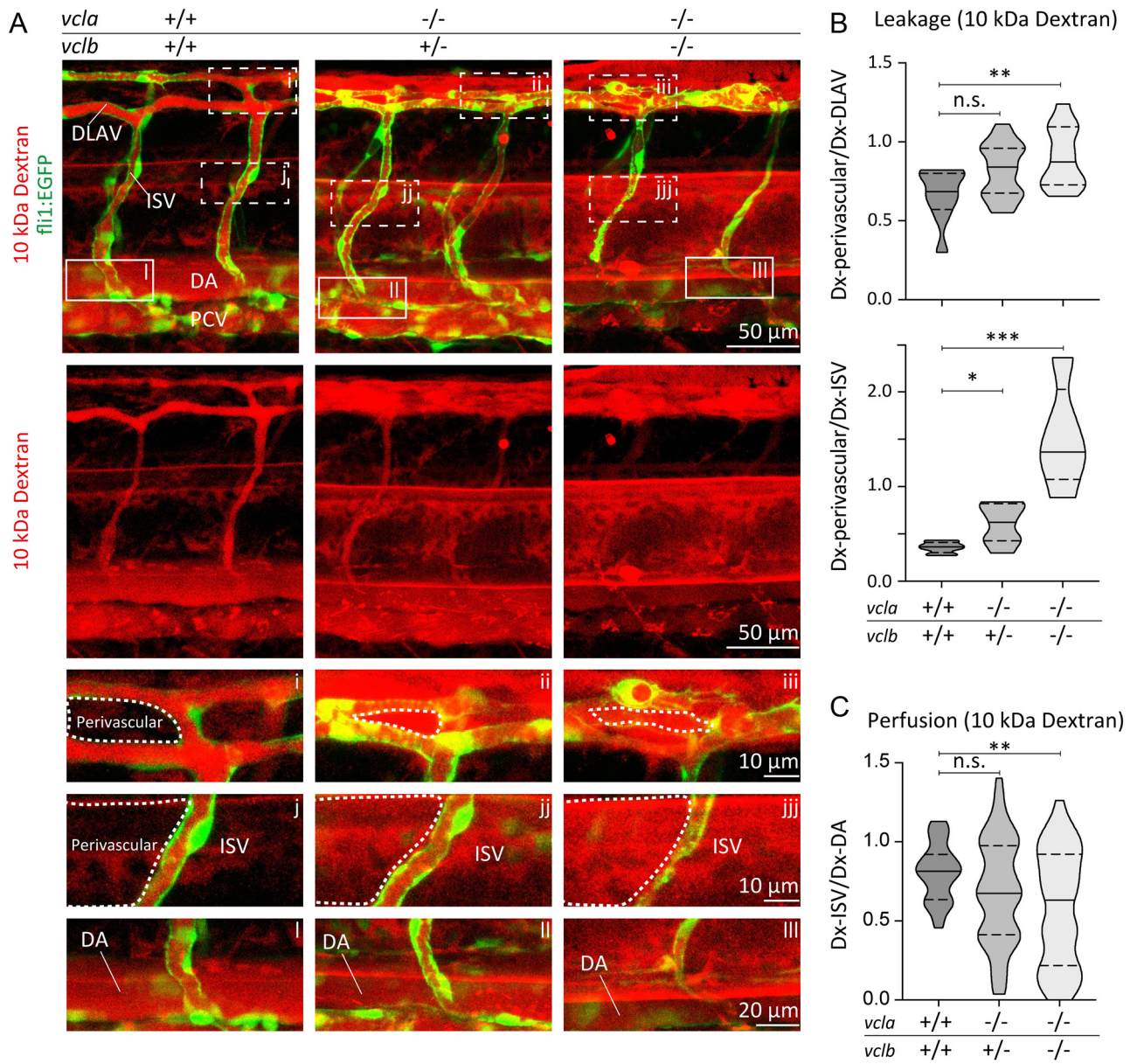


**Figure 2**

Vinculin ensures vascular barrier function for 10 kDa dextran. (A) Images of ISVs from 48 hpf Tg(*fli1:EGFP*) *vcla*$^{+/+}$;*vclb*$^{+/+}$, *vcla*$^{-/-}$;*vclb*$^{+/-}$ or *vcla*$^{-/-}$;*vclb*$^{-/-}$ embryos injected with 10 kDa rhodamine-dextran (red). Lower panels are single-channel images of the rhodamine signal. Scale bars, 50 µm. (A, i-iii) Corresponding close-up images showing the dextran leakage in the perivascular area around the dorsal longitudinal anastomotic vessel (DLAV). (A, j-jjj) Corresponding close-up images showing the dextran leakage in the perivascular area around an intersegmental vessel (ISV). Scale bars, 10 µm. (A, I-III) Close-up images of an ISV and the dorsal aorta (DA) showing the rhodamine signal within these vessels. Scale bar, 20 µm. (B) Violin plots showing the average leakage ± s.e. of 10 kDa dextran into the perivascular area of the DLAV or ISVs normalised to the dextran inside the DLAV or ISVs from 48 hpf embryos. The dotted lines represent the quartiles and the straight lines represent the median, $n$ = 10 *vcla*$^{+/+}$;*vclb*+/+, $n$ = 25 *vcla*$^{-/-}$;*vclb*$^{+/-}$ and $n$ = 13 *vcla*$^{-/-}$;*vclb*$^{-/-}$ embryos, n.s., non-significant, $^{*}P < 0.05$, $^{**}P < 0.01$, $^{***}P < 0.001$ (one-way ANOVA and Dunnett's post-test). PCV, posterior cardinal vein. (C) Violin plot showing the ISV perfusion determined as the ratio between fluorescent dextran levels inside the ISV ± s.e. and dextran inside the dorsal aorta (DA) from 48 hpf embryos. The dotted lines represent the quartiles, the straight lines represent the median. $n$ = 10 *vcla*$^{+/+}$;*vclb*$^{+/+}$, $n$ = 25 *vcla*$^{-/-}$;*vclb*$^{+/-}$ and $n$ = 13 *vcla*$^{-/-}$;*vclb*$^{-/-}$ embryos.

after microinjections. For visualisation of vascular leakage, embryos were mounted in 0.7% low-melting-point agarose (Sigma) and imaged with the Zeiss Axioplan Airy (25× oil/0.8 NA objective, confocal mode).

## Imaging and image analysis

Fixed HUVECs were imaged using widefield microscopy on a NIKON Eclipse TI, with a SOLA SE II light source, 60× 1.49

https://vb.bioscientifica.com
https://doi.org/10.1530/VB-22-0012

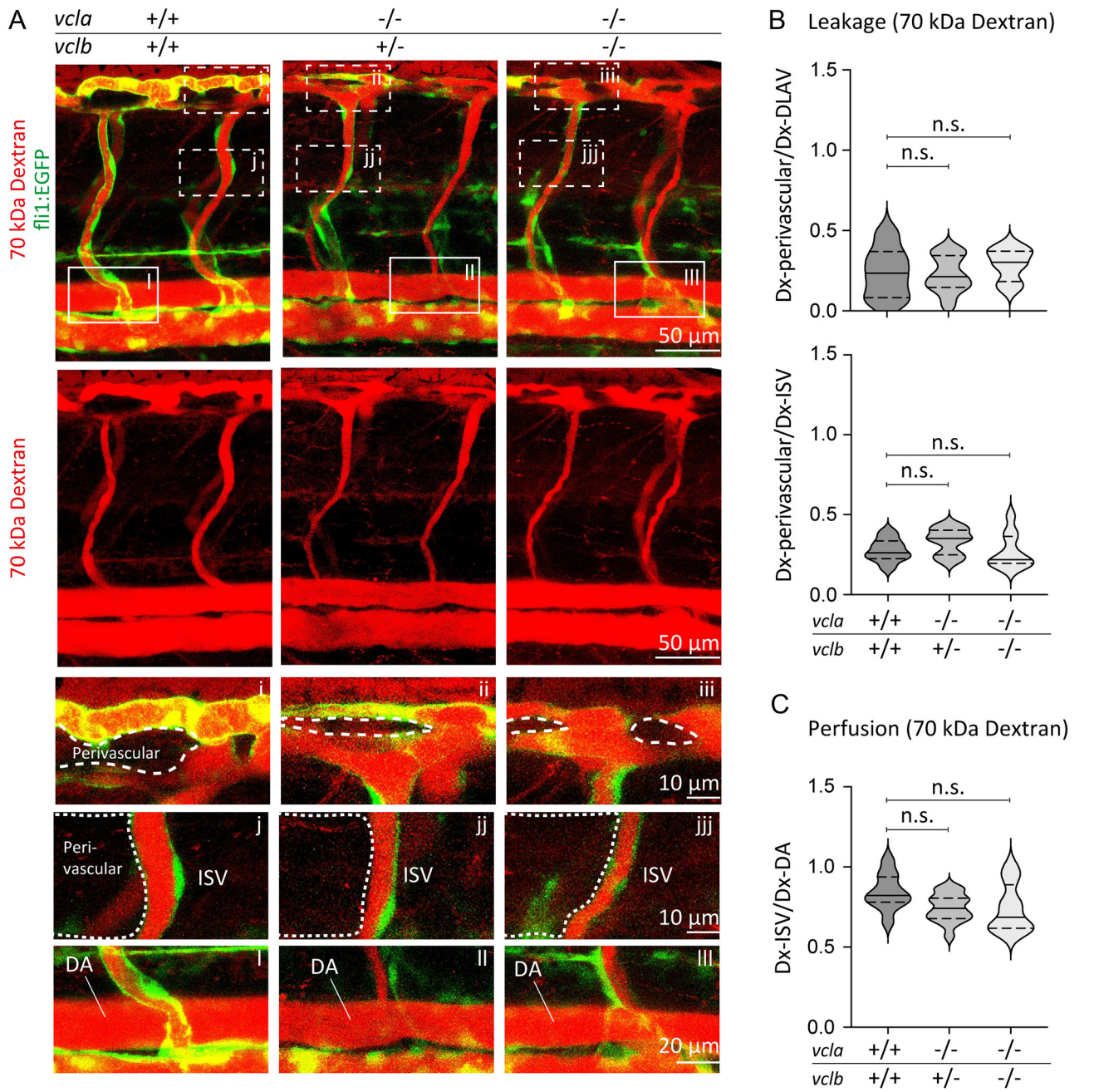


**Figure 3**

Loss of vinculin does not impair vascular barrier function for 70 kDa dextran. (A) Images of ISVs from 48 hpf Tg(*fli1:EGFP*) *vcla*$^{+/+}$;*vclb*$^{+/+}$, *vcla*$^{-/-}$;*vclb*$^{+/-}$ or *vcla*$^{-/-}$;*vclb*$^{-/-}$ embryos injected with 70 kDa rhodamine-dextran (red). Lower panels are single channel images of the rhodamine signal. Scale bars, 50 µm. (A, i-iii) Corresponding close-up images showing the dextran levels in the perivascular area around the dorsal longitudinal anastomotic vessel (DLAV). (A, j-jjj) Corresponding close-up images showing the dextran levels in the perivascular area around an intersegmental vessel (ISV). Scale bars, 10 µm. (A, I-III) Close-up images of an ISV and the dorsal aorta (DA) showing the rhodamine signal within these vessels. Scale bar, 20 µm. (B) Violin plot showing the average leakage ± S.E. of 70 kDa dextran into the perivascular area of the DLAV or ISVs normalised to the dextran inside the DLAV or ISVs from 48 hpf embryos. The dotted lines represent the quartiles, the straight lines represent the median, $n = 7$ *vcla*$^{+/+}$;*vclb*$^{+/+}$, $n = 16$ *vcla*$^{-/-}$;*vclb*$^{+/-}$ and $n = 7$ *vcla*$^{-/-}$;*vclb*$^{-/-}$ embryos, n.s. non-significant, one-way ANOVA and Dunnett's post-test. (C) Violin plot showing the ISV perfusion determined as the ratio between fluorescent dextran levels inside the ISV ± S.E. and dextran inside the dorsal aorta (DA) from 48 hpf embryos. The dotted lines represent the quartiles, the straight lines represent the median, $n = 10$ *vcla*$^{+/+}$;*vclb*$^{+/+}$, $n = 16$ *vcla*$^{-/-}$;*vclb*$^{+/-}$ and $n = 8$ *vcla*$^{-/-}$;*vclb*$^{-/-}$ embryos.

https://vb.bioscientifica.com
https://doi.org/10.1530/VB-22-0012

NA Apo TIRF (oil) objective and Andor Zyla 4.2 plus sCMOS camera and standard CFP, GFP or mCherry filter cubes (NIKON). For live imaging of zebrafish, a Zeiss LSM880 Airyscan inverted confocal microscope, with a 25× 0.8 NA oil objective was used. First, live embryos were selected for fluorescence signal and subsequently anaesthetised with 1× tricaine (0.08%) in E3 fish water and mounted in glass bottom Petri dishes (MatTek) using 0.7% low-melting-point agarose (Sigma) containing 1× tricaine. For live imaging, E3 with 1× tricaine and 0.003% 1-phenyl-2-thiourea (PTU, Sigma) was added to avoid pigmentation. Images were acquired with a zoom of 1–1.6 and z-stack step size of 0.5–1.0 µm, with a time interval of 25–30 min. Vascular perfusion and vascular leakage were analysed based on the fluorescent dextran levels in zebrafish embryos at 48 hpf. Vascular perfusion was defined as the ratio of fluorescent dextran levels in the ISVs to the levels of dextran inside the dorsal aorta (DA). Vascular leakage was defined as the ratio of the dextran fluorescent levels at the perivascular area of the vessels to the dextran levels inside the vessels. For this analysis, DLAV and its perivascular areas were analysed.

### Statistical analysis

Graphpad Prism was used for the statistical analysis of the data. All violin plots represent data distribution, with the dashed line representing the quartiles and the straight line representing the median. When two groups were compared, a Wilcoxon test was used. When two or more groups were compared to the control, a one-way ANOVA was used, in combination with Tukey's or Dunnett's post hoc test for multiple comparisons and a D'Agostino–Pearson test for normality. Asterisks indicate *P* values and are defined as n.s., non-significant, * $P<0.05$, ** $P<0.01$, *** $P<0.001$.

## Results

### Junctional vinculin strengthens the endothelial barrier *in vitro*

Vinculin is recruited to tensile AJs by α-catenin. In addition, vinculin localises at integrin-based focal adhesions (FAs) through its force-dependent interaction with talin (36). To specifically investigate the role of junctional vinculin, we used lentiviral shRNA transductions that deplete endogenous α-catenin from human umbilical vein endothelial cells (HUVECs). Subsequently, we lentivirally expressed mouse α-catenin–GFP (green fluorescent protein) or α-catenin–ΔVBS–GFP, a modified α-catenin protein in which the binding to vinculin is prevented (22). Western blot analysis confirmed the depletion of endogenous α-catenin and expression of the α-catenin–GFP and α-catenin–ΔVBS–GFP in the rescued cells (Fig. 1A). Immunofluorescent (IF) stainings for VE–cadherin were performed to assess AJs in the different experimental conditions. Knockdown of α-catenin led to disassembly of AJs. The expression of α-catenin–GFP and α–catenin–ΔVBS–GFP restored the AJs in shα–catenin HUVECs (Fig. 1B), as shown previously (22). Next, we examined junctional vinculin recruitment by performing IF analysis. Vinculin localised at both FAs and AJs in wild type α-catenin rescued HUVECs (Fig. 1C and D). Analysis of α-catenin–ΔVBS-based junctions showed efficient preclusion of vinculin from the tensile AJs, while vinculin localisation at the FAs was maintained (Fig. 1C and D). This confirms the junction-specific depletion of vinculin in the α-catenin–ΔVBS-expressing cells. To examine whether junctional vinculin controls endothelial barrier function, we next performed electric cell-substrate impedance sensing (ECIS) as readout for the tightness of the endothelial cell monolayers. Silencing of endogenous α-catenin expression led to a decrease in transendothelial resistance, indicating an impairment of endothelial barrier function (Fig. 1E). Restoring α-catenin levels by α-catenin–GFP re-established endothelial monolayer integrity; however, α–catenin–ΔVBS–GFP expression, the mutated form lacking the vinculin binding site did not fully restore barrier function (Fig. 1E and F). To investigate whether the junctional depletion of vinculin might affect barrier loss upon physiological remodelling conditions, we performed ECIS experiments following treatment with the permeability factor Thrombin. These experiments showed that thrombin-induced barrier loss occurs similarly in α-catenin–GFP or α-catenin–ΔVBS–GFP rescued endothelial monolayers (Fig. 1G). Taken together, these results indicate that junctional vinculin promotes basal endothelial barrier function.

### Vinculin mediates vascular barrier function for small molecules

Since junctional vinculin strengthens the barrier function of cultured endothelial monolayers, we next investigated the consequence of vinculin ablation on the vascular barrier *in vivo*. We recently showed that vinculin is important for the formation of junctional fingers in response to blood flow in the developing vessels of zebrafish (34). The zebrafish genome encodes two vinculin isoforms, vinculin a (*vcla*) and vinculin

https://vb.bioscientifica.com
https://doi.org/10.1530/VB-22-0012

b (*vclb*) (37, 38). The genetic ablation of both vinculin isoforms delays sprouting angiogenesis during early vascular development (34). Nevertheless, the *vcl*-KO embryos develop functional blood vessels and no evident haemorrhages were observed (34). To assess the permeability of the endothelial barrier, the 10 kDa rhodamine-dextran tracer was injected into the duct of Cuvier at 48 hpf of control or *vcl*-KO Tg(*fli1a:EGFP*)$^{y1}$ embryos, in which the *fli1a* promoter drives the endothelial-specific expression of EGFP. One hour after dextran-microinjections, we examined vascular perfusion and leakage by imaging the blood vessels of the zebrafish trunk, namely the intersegmental vessels (ISVs), the DLAV and their perivascular areas. The ISVs of control embryos were perfused, as shown by the presence of the 10 kDa rhodamine-dextran tracer in the lumen of blood vessels. In control zebrafish, the tracer was maintained in the blood vessel lumen of the DLAV and the ISVs and did not extravasate into the perivascular regions (Fig. 2A-C), which indicates that endothelial junctions are sufficiently tight to prevent leakage of small molecular such as 10 kDa rhodamine-dextran. Conversely, in *vcl* mutants, we observed extensive leakage of the tracer dye into the surrounding tissues (Fig. 2A and B). In *vcla*$^{-/-}$*;vclb*$^{+/-}$, and in particular, in *vcl* full-KO embryos, the 10 kDa rhodamine-dextran intensities were lower within the perfused ISVs, suggesting that dextran molecules extravasated from the circulation (Fig. 2C). Our analysis shows that *vcla*$^{-/-}$*; vclb*$^{+/-}$ and *vcl* full-KO embryos exhibited increased perivascular dextran levels (Fig. 2A and B). To examine the requirement of vinculin for vascular barrier function of larger molecules, we next injected 70 kDa rhodamine-dextran in *fli1:EGFP* control and *vcl* KO embryos. An hour after dextran-microinjections, no differences in vascular permeability and perfusion between control and *vcl* heterozygous or homozygous KO embryos were observed (Fig. 3A-C). Taken together, these experiments demonstrate that vinculin is required for the strengthening of the endothelial barrier in newly developed blood vessels to prevent leakage of small molecules.

## Discussion

Endothelial barrier function is tightly regulated through force-dependent remodelling of cell–cell contacts. Failure of the endothelial junctions to adapt to subjected forces leads to vascular leakage and inflammation in cardiovascular disease (1). In this study, we examined the importance of the mechanotransduction protein vinculin for the endothelial barrier using both *in vitro* and *in vivo* functional approaches. These results reveal that recruitment of vinculin to AJs strengthens the endothelial cell–cell junctions in blood vessels.

Vinculin knockout mice are embryonically lethal due to neuronal and cardiovascular defects at E10.5 (39), demonstrating the importance of vinculin for mammalian development. In addition, endothelial-specific vinculin depletion constrains collective endothelial migration during retinal angiogenesis in mice (35), indicating that endothelial vinculin contributes to vascular development. Endothelial vinculin is recruited to both integrin-based FAs and cadherin-based AJs in a force-dependent manner (29, 36). When tensile forces remodel AJs, vinculin-mediated mechanotransduction occurs via the VE–cadherin complex (22). By generating endothelial cells that form junctions through the vinculin-binding-deficient α-catenin mutant (α-catenin–ΔVBS), we now specifically showed that junctional vinculin recruitment supports strengthening of monolayer integrity in cultured endothelial cells. Single *vcla* or *vclb* mutant zebrafish display mild developmental defects (38, 40). We find that the *vcla*$^{-/-}$*;vclb*$^{-/-}$ double knockout zebrafish exhibit mild defects in vascular morphogenesis and eventually the morphogenetic process gives rise to a functional vasculature (34). In line with the expectation that vinculin modulates, rather than being needed for, endothelial cell–cell junctions (22, 27, 28), we observed vascular leakage specifically for small molecules, 10 kDa, in vinculin knockout zebrafish, whereas the vasculature still acted as a barrier for larger molecules. This result is corroborated by the notion that recruitment of vinculin to VE–cadherin-based junctions does not affect histamine-induced vascular leakage of Evans Blue in mice, which is a measure for the extravasation of large molecules (27). Even though the measured resistance formed by cultured endothelial cells expressing α-catenin–ΔVBS indicated minor barrier differences upon the junctional depletion of vinculin, the knockout of vinculin in vivo resulted in significant leakage of small molecules. This indicates that the endothelial dysfunction upon vinculin depletion becomes aggravated in pressurised vascular conditions. Potentially, the mild phenotype of the vinculin knockout zebrafish might be aggravated under pathological conditions that weaken the endothelial barrier, such as during inflammation or sepsis. Together, the data show that vinculin tightens endothelial junctions in blood vessels.

We expect that the depletion of the junctional vinculin pool underlies the vascular phenotype of the vinculin KO zebrafish. Cultured endothelial cells that form junctions through α-catenin–ΔVBS fail to sprout in collagen gels

https://vb.bioscientifica.com
https://doi.org/10.1530/VB-22-0012

(data not shown). This suggests that the junctional pool of vinculin controls endothelial dynamics within angiogenic sprouts, an effect that has also been observed in endothelial-specific knockout mice (35). Moreover, we recently observed differences in flow-induced endothelial junction dynamics in the ISVs of control and vinculin KO zebrafish, whereas integrin-dependent filopodia still formed equally (34). Other groups showed that juvenile *Vclb*-mutant zebrafish display epicardial defects and pericardial edema (38, 40, 41). Recruitment of vinculin was observed during the maturation of cell–cell junctions between cardiomyocytes in vivo (41). These findings suggest that *in vivo,* vinculin's role in cell–cell junctions is prominent. Nevertheless, a potential contribution of vinculin's role in integrin-based adhesion cannot be fully ruled out in this model system.

Finally, we surmise that junctional vinculin recruitment fortifies the endothelial barrier for small molecules upon vascular remodelling. Future work targeting the protective function of vinculin using pharmacological approaches, for instance by enhancing its interaction with the junctions, may provide a strategy to treat pathologies that entail vascular permeability.

**Declaration of interest**

The authors declare that there is no conflict of interest.

**Funding**

This work has been supported by the Kantons Basel-Stadt and Basel-Land and by a grant from the Swiss National Science Foundation to M.A.. S.H. is financially supported by the Netherlands Organization of Scientific Research (ZonMw VIDI grant 016.156.327) and the Rembrandt Institute for Cardiovascular Sciences. M.S. was financially supported by (EUFish, UvA365, Amsterdam UMC).

**Author contribution statement**

MvdS, MK and RS designed and performed experiments. SH and HGB conceived and supervised the study. MvdS, MK, RS, HGB and SH analysed the data. MvdS, MK, HGB and SH wrote the manuscript. All authors reviewed the manuscript.

**Data availability**

Data are available from the authors upon reasonable request.

## References

1 Claesson-Welsh L, Dejana E & McDonald DM. Permeability of the endothelial barrier: identifying and reconciling controversies. *Trends in Molecular Medicine* 2021 **27** 314–331. (https://doi.org/10.1016/j.molmed.2020.11.006)

2 Wettschureck N, Strilic B & Offermanns S. Passing the vascular barrier: endothelial signaling processes controlling extravasation. *Physiological Reviews* 2019 **99** 1467–1525. (https://doi.org/10.1152/physrev.00037.2018)

3 Schimmel L, Heemskerk N & van Buul JD. Leukocyte transendothelial migration: a local affair. *Small GTPases* 2017 **8** 1–15. (https://doi.org/10.1080/21541248.2016.1197872)

4 Weis SM & Cheresh DA. Pathophysiological consequences of VEGF-induced vascular permeability. *Nature* 2005 **437** 497–504. (https://doi.org/10.1038/nature03987)

5 Radeva MY & Waschke J. Mind the gap: mechanisms regulating the endothelial barrier. *Acta Physiologica* 2018 **222** e12860. (https://doi.org/10.1111/apha.12860)

6 Liu HB, Zhang J, Xin SY, Liu C, Wang CY, Zhao D & Zhang ZR. Mechanosensitive properties in the endothelium and their roles in the regulation of endothelial function. *Journal of Cardiovascular Pharmacology* 2013 **61** 461–470. (https://doi.org/10.1097/FJC.0b013e31828c0933)

7 Hahn C & Schwartz MA. Mechanotransduction in vascular physiology and atherogenesis. *Nature Reviews. Molecular Cell Biology* 2009 **10** 53–62. (https://doi.org/10.1038/nrm2596)

8 Dessalles CA, Leclech C, Castagnino A & Barakat AI. Integration of substrate- and flow-derived stresses in endothelial cell mechanobiology. *Communications Biology* 2021 **4** 764. (https://doi.org/10.1038/s42003-021-02285-w)

9 Phng LK & Belting HG. Endothelial cell mechanics and blood flow forces in vascular morphogenesis. *Seminars in Cell and Developmental Biology* 2021 **120** 32–43. (https://doi.org/10.1016/j.semcdb.2021.06.005)

10 Dorland YL & Huveneers S. Cell–cell junctional mechanotransduction in endothelial remodeling. *Cellular and Molecular Life Sciences* 2017 **74** 279–292. (https://doi.org/10.1007/s00018-016-2325-8)

11 Dejana E, Orsenigo F & Lampugnani MG. The role of adherens junctions and VE-cadherin in the control of vascular permeability. *Journal of Cell Science* 2008 **121** 2115–2122. (https://doi.org/10.1242/jcs.017897)

12 Dejana E & Vestweber D. The role of VE-cadherin in vascular morphogenesis and permeability control. *Progress in Molecular Biology and Translational Science* 2013 **116** 119–144. (https://doi.org/10.1016/B978-0-12-394311-8.00006-6)

13 Cao J, Ehling M, März S, Seebach J, Tarbashevich K, Sixta T, Pitulescu ME, Werner AC, Flach B, Montanez E *et al.* Polarized actin and VE-cadherin dynamics regulate junctional remodelling and cell migration during sprouting angiogenesis. *Nature Communications* 2017 **8** 2210. (https://doi.org/10.1038/s41467-017-02373-8)

14 Bentley K, Franco CA, Philippides A, Blanco R, Dierkes M, Gebala V, Stanchi F, Jones M, Aspalter IM, Cagna G *et al.* The role of differential VE-cadherin dynamics in cell rearrangement during angiogenesis. *Nature Cell Biology* 2014 **16** 309–321. (https://doi.org/10.1038/ncb2926)

15 Angulo-Urarte A, van der Wal T & Huveneers S. Cell-cell junctions as sensors and transducers of mechanical forces. *Biochimica et Biophysica Acta. Biomembranes* 2020 **1862** 183316. (https://doi.org/10.1016/j.bbamem.2020.183316)

16 Pannekoek W-J, de Rooij J & Gloerich M. Force transduction by cadherin adhesions in morphogenesis. *F1000Research* 2019 **8** F1000. (https://doi.org/10.12688/f1000research.18779.1)

17 Mège RM & Ishiyama N. Integration of cadherin adhesion and cytoskeleton at adherens junctions. *Cold Spring Harbor Perspectives in Biology* 2017 **9** a028738. (https://doi.org/10.1101/cshperspect.a028738)

18 Charras G & Yap AS. Tensile forces and mechanotransduction at cell–cell junctions. *Current Biology* 2018 **28** R445–R457. (https://doi.org/10.1016/j.cub.2018.02.003)

19 Buckley CD, Tan J, Anderson KL, Hanein D, Volkmann N, Weis WI, Nelson WJ & Dunn AR. Cell adhesion. The minimal cadherin-catenin complex binds to actin filaments under force. *Science* 2014 **346** 1254211. (https://doi.org/10.1126/science.1254211)

20 Noda K, Zhang J, Fukuhara S, Kunimoto S, Yoshimura M & Mochizuki N. Vascular endothelial-cadherin stabilizes at cell-cell junctions by anchoring to circumferential actin bundles through alpha- and beta-catenins in cyclic AMP-Epac-Rap1 signal-activated endothelial cells. *Molecular Biology of the Cell* 2010 **21** 584–596. (https://doi.org/10.1091/mbc.e09-07-0580)

21 Schulte D, Küppers V, Dartsch N, Broermann A, Li H, Zarbock A, Kamenyeva O, Kiefer F, Khandoga A, Massberg S *et al.* Stabilizing the VE-cadherin-catenin complex blocks leukocyte extravasation and vascular permeability. *EMBO Journal* 2011 **30** 4157–4170. (https://doi.org/10.1038/emboj.2011.304)

22 Huveneers S, Oldenburg J, Spanjaard E, van der Krogt G, Grigoriev I, Akhmanova A, Rehmann H & de Rooij J. Vinculin associates with endothelial VE-cadherin junctions to control force-dependent remodeling. *Journal of Cell Biology* 2012 **196** 641–652. (https://doi.org/10.1083/jcb.201108120)

23 Liu Z, Tan JL, Cohen DM, Yang MT, Sniadecki NJ, Ruiz SA, Nelson CM & Chen CS. Mechanical tugging force regulates the size of cell-cell junctions. *Proceedings of the National Academy of Sciences of the United States of America* 2010 **107** 9944–9949. (https://doi.org/10.1073/pnas.0914547107)

24 Yonemura S, Wada Y, Watanabe T, Nagafuchi A & Shibata M. α-Catenin as a tension transducer that induces adherens junction development. *Nature Cell Biology* 2010 **12** 533–542. (https://doi.org/10.1038/ncb2055)

25 le Duc Q, Shi Q, Blonk I, Sonnenberg A, Wang N, Leckband D & de Rooij J. Vinculin potentiates E-cadherin mechanosensing and is recruited to actin-anchored sites within adherens junctions in a myosin II–dependent manner. *Journal of Cell Biology* 2010 **189** 1107–1115. (https://doi.org/10.1083/jcb.201001149)

26 Ishiyama N, Sarpal R, Wood MN, Barrick SK, Nishikawa T, Hayashi H, Kobb AB, Flozak AS, Yemelyanov A, Fernandez-Gonzalez R *et al.* Force-dependent allostery of the α-catenin actin-binding domain controls adherens junction dynamics and functions. *Nature Communications* 2018 **9** 5121. (https://doi.org/10.1038/s41467-018-07481-7)

27 Duong CN, Brückner R, Schmitt M, Nottebaum AF, Braun LJ, zu Brickwedde MM, Ipe U, Vom Bruch H, Schöler HR, Trapani G *et al.* Force-induced changes of α-catenin conformation stabilize vascular junctions independent of vinculin. *Journal of Cell Science* 2021 **134**. (https://doi.org/10.1242/jcs.259012)

28 Twiss F, Le Duc Q, Van Der Horst S, Tabdili H, Van Der Krogt G, Wang N, Rehmann H, Huveneers S, Leckband DE & De Rooij J. Vinculin-dependent cadherin mechanosensing regulates efficient epithelial barrier formation. *Biology Open* 2012 **1** 1128–1140. (https://doi.org/10.1242/bio.20122428)

29 Yao M, Qiu W, Liu R, Efremov AK, Cong P, Seddiki R, Payre M, Lim CT, Ladoux B, Mège RM *et al.* Force-dependent conformational switch of α-catenin controls vinculin binding. *Nature Communications* 2014 **5** 4525. (https://doi.org/10.1038/ncomms5525)

30 Seddiki R, Narayana GHNS, Strale PO, Balcioglu HE, Peyret G, Yao M, Le AP, Teck Lim C, Yan J, Ladoux B *et al.* Force-dependent binding of vinculin to α-catenin regulates cell-cell contact stability and collective cell behavior. *Molecular Biology of the Cell* 2018 **29** 380–388. (https://doi.org/10.1091/mbc.E17-04-0231)

31 Barry AK, Wang N & Leckband DE. Local VE-cadherin mechanotransduction triggers long-ranged remodeling of endothelial monolayers. *Journal of Cell Science* 2015 **128** 1341–1351. (https://doi.org/10.1242/jcs.159954)

32 Birukova AA, Shah AS, Tian Y, Moldobaeva N & Birukov KG. Dual role of vinculin in barrier-disruptive and barrier-enhancing endothelial cell responses. *Cellular Signalling* 2016 **28** 541–551. (https://doi.org/10.1016/j.cellsig.2016.02.015)

33 Kugelmann D, Rotkopf LT, Radeva MY, Garcia-Ponce A, Walter E & Waschke J. Histamine causes endothelial barrier disruption via Ca2+-mediated RhoA activation and tension at adherens junctions. Sci Rep. *Scientific Reports* 2018 **8** 13229. (https://doi.org/10.1038/s41598-018-31408-3)

34 Kotini MP, van der Stoel MM, Yin J, Han MK, Kirchmaier B, de Rooij J, Affolter M, Huveneers S & Belting HG. Vinculin controls endothelial cell junction dynamics during vascular lumen formation. *Cell Reports* 2022 **39** 110658. (https://doi.org/10.1016/j.celrep.2022.110658)

35 Carvalho JR, Fortunato IC, Fonseca CG, Pezzarossa A, Barbacena P, Dominguez-Cejudo MA, Vasconcelos FF, Santos NC, Carvalho FA & Franco CA. Non-canonical Wnt signaling regulates junctional mechanocoupling during angiogenic collective cell migration. *eLife* 2019 **8** e45853. (https://doi.org/10.7554/eLife.45853)

36 Yao M, Goult BT, Chen H, Cong P, Sheetz MP & Yan J. Mechanical activation of vinculin binding to talin locks talin in an unfolded conformation. *Scientific Reports* 2014 **4** 4610. (https://doi.org/10.1038/srep04610)

37 Pascoal S, Esteves de Lima J, Leslie JD, Hughes SM & Saúde L. Notch signalling is required for the formation of structurally stable muscle fibres in zebrafish. *PLOS ONE* 2013 **8** e68021. (https://doi.org/10.1371/journal.pone.0068021)

38 Han MKL, van der Krogt GNM & de Rooij J. Zygotic vinculin is not essential for embryonic development in zebrafish. *PLoS One* 2017 **12** e0182278. (https://doi.org/10.1371/journal.pone.0182278)

39 Xu W, Baribault H & Adamson ED. Vinculin knockout results in heart and brain defects during embryonic development. *Development* 1998 **125** 327–337. (https://doi.org/10.1242/dev.125.2.327)

40 Cheng F, Miao L, Wu Q, Gong X, Xiong J & Zhang J. Vinculin b deficiency causes epicardial hyperplasia and coronary vessel disorganization in zebrafish. *Development* 2016 **143** 3522–3531. (https://doi.org/10.1242/dev.132936)

41 Fukuda R, Gunawan F, Ramadass R, Beisaw A, Konzer A, Mullapudi ST, Gentile A, Maischein HM, Graumann J & Stainier DYR. Mechanical forces regulate cardiomyocyte myofilament maturation via the VCL-SSH1-CFL axis. *Developmental Cell* 2019 **51** 62–77.e5. (https://doi.org/10.1016/j.devcel.2019.08.006)

42 van der Stoel M, Schimmel L, Nawaz K, van Stalborch AM, de Haan A, Klaus-Bergmann A, Valent ET, Koenis DS, van Nieuw Amerongen GP, de Vries CJ *et al.* DLC1 is a direct target of activated YAP/TAZ that drives collective migration and sprouting angiogenesis. *Journal of Cell Science* 2020 **133** jcs239947. (https://doi.org/10.1242/jcs.239947)

43 Dorland YL, Malinova TS, van Stalborch AM, Grieve AG, van Geemen D, Jansen NS, de Kreuk BJ, Nawaz K, Kole J, Geerts D *et al.* The F-BAR protein pacsin2 inhibits asymmetric VE-cadherin internalization from tensile adherens junctions. *Nature Communications* 2016 **7** 12210. (https://doi.org/10.1038/ncomms12210)

44 Aleström P, D'Angelo L, Midtlyng PJ, Schorderet DF, Schulte-Merker S, Sohm F & Warner S. Zebrafish: housing and husbandry recommendations. *Laboratory Animals* 2020 **54** 213–224. (https://doi.org/10.1177/0023677219869037)

45 Lawson ND & Weinstein BM. In vivo imaging of embryonic vascular development using transgenic zebrafish. *Developmental Biology* 2002 **248** 307–318. (https://doi.org/10.1006/dbio.2002.0711)

46 Meeker ND, Hutchinson SA, Ho L & Trede NS. Method for isolation of PCR-ready genomic DNA from zebrafish tissues. *BioTechniques* 2007 **43** 610–614. (https://doi.org/10.2144/000112619)

47 Lenard A, Ellertsdottir E, Herwig L, Krudewig A, Sauteur L, Belting HG & Affolter M. In vivo analysis reveals a highly stereotypic morphogenetic pathway of vascular anastomosis. *Developmental Cell* 2013 **25** 492–506. (https://doi.org/10.1016/j.devcel.2013.05.010)

48 Weinstein BM, Stemple DL, Driever W & Fishman MC. Gridlock, a localized heritable vascular patterning defect in the zebrafish. *Nature Medicine* 1995 **1** 1143–1147. (https://doi.org/10.1038/nm1195-1143)


Received 12 May 2022
Accepted 19 October 2022
Available online 19 October 2022
Version of Record published 27 January 2023